An Iron-Based Molecular Redox Switch as a Model for Iron Release from Enterobactin via the Salicylate Binding Mode

Thomas R. Ward,*,† Andreas Lutz,† Serge P. Parel,† Jürgen Ensling,‡ Philipp Gütlich,‡ Péter Buglyó,§ and Chris Orvig§

Department of Chemistry and Biochemistry, University of Berne, Freiestrasse 3, CH-3012 Berne, Switzerland, Institut für Anorganische und Analytische Chemie, Johannes Gutenberg-Universität Mainz, Staudingerweg 9, D-55099 Mainz, Germany, and Department of Chemistry, University of British Columbia, 2036 Main Mall, Vancouver, British Columbia, Canada V6T 1Z1

Received February 24, 1999

The iron release mechanism from protonated ferric enterobactin [Fe^{III}(enterobactinH_3)] via the salicylate binding mode was probed. For this purpose, a tripodal dodecadentate ligand incorporating three salicylamide (**OO**) and three bipyridine (**NN**) binding sites was synthesized as well as iron complexes thereof. It was shown that a ferric ion coordinates selectively to the hard salicylamides and a ferrous ion binds to the softer bipyridines. Upon reduction or oxidation, the iron translocates reversibly and intramolecularly from one site to the other, thus displaying switchlike properties. Both states were characterized by cyclic voltammetry and visible and Mössbauer spectroscopy. The Mössbauer spectrum for the ferric complex is fully consistent with that obtained by Pecoraro et al. upon lowering the pH of [Fe^{III}(enterobactin)]$^{3-}$ solutions (Pecoraro, V. L., et al. *J. Am. Chem. Soc.* **1983**, *105*, 4617), thus supporting the alternative iron release mechanism from enterobactin via the salicylate binding mode.

Introduction

For virtually all organisms, life without iron would be impossible. As both iron deficiency and iron excess are detrimental, understanding the iron uptake and iron storage mechanism is crucial.[1,2]

Many siderophores (high-affinity iron sequestering agents) possess either triscatechol or trishydroxamate binding sites, and more than 300 naturally occurring ferric ion scavengers have been isolated and characterized to date.[3] Much effort has been invested in the synthesis of both natural and synthetic siderophores, eventually leading to the commercialization of desferrioxamine, administered in case of iron poisoning.[4]

To overcome the low solubility of iron hydroxides present in seawater from which contemporary organisms are thought to have evolved, the siderophores possess very high binding constants toward Fe(III), often greater than the solubility product of $Fe(OH)_3$: $pK_{sp} = 36$. The naturally occurring triscatechol enterobactin is the most powerful natural iron(III) chelator known with an overall stability constant of $\approx 10^{49}$.[5] With such high affinity for Fe(III), the iron release mechanism remains controversial.[6] To date, three hypotheses have been put forward: (a) Fe(III) reduction,[7] (b) ligand hydrolysis,[8,9] and (c) ligand protonation.[10−13]

The reduction potentials of [Fe^{III}(hydroxamate)] at neutral pH are within the range of known biological reductants such as NADH or $FADH_2$ (Figure 1A). Upon reduction, the [Fe^{II}(hydroxamate)]$^-$ binding constant significantly decreases, thus allowing softer ligands to scavenge the ferrous ion from the hard hydroxamate chelate.[7] The reduction potential of [Fe^{III}(enterobactin)]$^{3-}$ at neutral pH, however, lies outside of the reducing power of these reductants. Another release mechanism must thus be operative. As the enterobactin backbone consists of a hydrolytically unstable trislactone macrocycle, it has been suggested that esterases may be responsible for the hydrolysis of the anchor, facilitating liberation of Fe^{3+} (Figure 1B).[8] It has been shown, however, that microorganisms are able to utilize iron supplied by enterobactin analogues lacking the trislactone backbone.[14] Although these synthetic siderophores are usually only 5% as effective in delivering iron to the cell, this is still sufficient to ensure significant growth.[15] This led to

† University of Bern.
‡ Johannes Gutenberg-Universität Mainz.
§ University of British Columbia.

(1) Theil, E. C.; Raymond, K. N. In *Bioinorganic Chemistry;* Bertini, I., Gray, H. B., Lippard, S. J., Valentine, J. S., Eds.; University Science Books: Mill Valley, CA, 1994; pp 1−37.
(2) For a recent and thorough review see *Metal Ions Biological Systems, Vol. 35: Iron Transport and Storage in Microorganisms, Plants and Animals*; Sigel, A., Sigel, H., Eds.; Marcel Dekker Inc.: Basel, Switzerland, 1998.
(3) Matzanke, B. F.; Müller-Matzanke, G.; Raymond, K. N. *Iron Carriers and Iron Proteins*; Loehr, T. M., Ed.; VCH: Weinheim, Germany, 1989; pp 1−121.
(4) Lippard, S. J.; Berg, J. M. *Principles of Bioinorganic Chemistry*; University Science Books: Mill Valley, CA, 1994.
(5) Loomis, L. D.; Raymond, K. N. *Inorg. Chem.* **1991**, *30*, 906.
(6) Crumbliss, A. L.; Batinic-Haberle, I.; Spasojevic, I. *Pure Appl. Chem.* **1996**, *68*, 1225.
(7) Hider, R. C. *Struct. Bonding* **1984**, *58*, 25.
(8) O'Brien, J. G.; Cox, G. B.; Gibson, F. *Biochim. Biophys. Acta* **1971**, *237*, 537.
(9) Brickman, T. J.; McIntosh, M. A. *J. Biol. Chem.* **1992**, *267*, 12350.
(10) Cass, M. E.; Garrett, T. M.; Raymond, K. N. *J. Am. Chem. Soc.* **1989**, *111*, 1677.
(11) Pecoraro, V. L.; Wong, G. B.; Kent, T. A.; Raymond, K. N. *J. Am. Chem. Soc.* **1983**, *105*, 4617.
(12) Raymond, K. N.; Cass, M. E.; Evans, S. L. *Pure Appl. Chem.* **1987**, *59*, 771.
(13) Pecoraro, V. L.; Harris, W. R.; Wong, G. B.; Carrano, C. J.; Raymond, K. N. *J. Am. Chem. Soc.* **1983**, *105*, 4623.
(14) Heidinger, S.; Braun, V.; Pecoraro, V. L.; Raymond, K. N. *J. Bacteriol.* **1983**, *153*, 109.

10.1021/ic990225e CCC: $18.00
Published on Web 10/13/1999

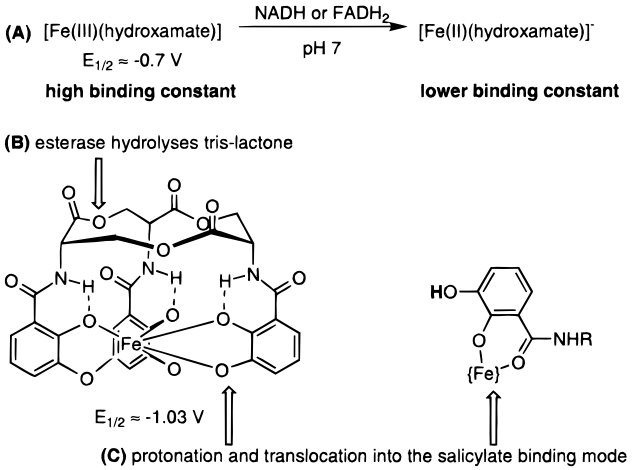

Figure 1. Three possible iron-release mechanisms from [Fe(siderophore)]: (A) reduction, (B) hydrolysis, and (C) protonation.

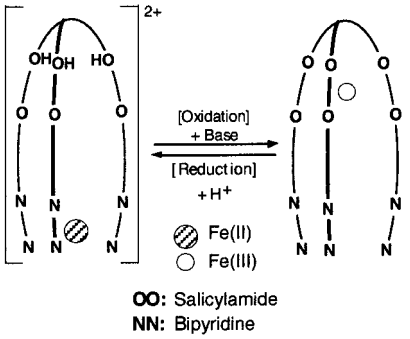

Figure 2. Redox-triggered reversible iron translocation in a tripodal dodecadentate ligand.

the proposal that iron release from $[Fe(enterobactin)]^{3-}$ in *Escherichia coli* may be facilitated by protonation of the catechol oxygen with subsequent translocation into the so-called salicylate binding mode (Figure 1C).[10−13] Until recently, the coordination properties of salicylamides have received only little attention in coordination chemistry.[16,17] Last year, Cohen et al.[15] published the first structural characterization of an $[Fe(salicylamide)_3]$-type complex.[15]

To probe the relevance of the salicylate binding mode in the iron release mechanism, we have synthesized a tripodal dodecadentate ligand incorporating three salicylamide moieties as well as three bipyridine moieties (abbreviated as **OO** and **NN**, respectively).[18,19] In the presence of a single iron, and depending on its oxidation state, we expect the iron to bind selectively to either one or the other octahedral site. By modifying the oxidation state, the metal ion should translocate from one binding site to the other, eventually leading to the development of a redox-triggered molecular switch (or shuttle), as illustrated in Figure 2.

In recent years, interest in molecular devices[20] has yielded several transition-metal based redox-triggered molecular switches.[21]

After initiation of this project, Shanzer and co-workers[22] published an outstanding report on a molecular switch based on the redox-triggered iron translocation in heteroditopic ligands incorporating bipyridine- and hydroxamate-binding sites.[22] This system can be regarded as a model for the iron release from hydroxamate-containing siderophores via a reduction pathway. Along similar lines, they reported a calix-[4]-arene-based system incorporating two hydroxamate binding sites and two bipyridines.[22c] More recently Pierre and co-workers[23] reported a bicompartmental ligand with one harder and one softer cavity that, when in the presence of a single iron ion, displays redox-triggered switching properties. In their system the iron remains bound to a phenolic oxygen during translocation, ensuring an intramolecular switching process.

Copper-based redox switches have been investigated by Sauvage's group as well as Zahn and Canary.[24] In these systems, the oxidation of Cu(I) to Cu(II) induces a reversible change in coordination number from four to five. Sauvage's systems exploits the electrochemically induced swinging of a [2]-catenane that incorporates terpyridine as well as phenanthroline-binding units.[24a,b] Zahn and Canary's system relies on the association/dissociation of a quinoline arm of a trisquinolylamine upon copper oxidation/reduction.[24c]

Fabrizzi and co-workers[25] reported a multicomponent coordination compound incorporating two nickel centers and one copper center that exhibits reversible electrochemically triggered anionic ligand translocation from copper to nickel.

As outlined above, the molecular switch presented herein was designed to probe the iron release mechanism from enterobactin via a salicylate binding mode.

Synthesis and Characterization. The synthesis of the tripodal dodecadentate ligand **6** is presented in Figure 3. Bromoester **1** reacts smoothly with Me_3TREN, $N(CH_2CH_2NHMe)_3$, to afford the trisamine **2**. Heating **2** in neat 1,2-diaminoethane nearly quantitatively yields the trisaminoamide **3**. In the presence of triethylamine in DMF, slow addition of 2,2′-bipyridine acid chloride **4** to trisaminoamide **3** affords the MOM-protected tripod **5**. Acetal cleavage, catalyzed by HCl, yields the dodecadentate ligand **6** in 18% overall yield.[18]

For model studies, structurally related tripodal hexadentate ligands incorporating *only* either the bipyridine- (**NN**) or the salicylamide-binding sites (**OO**) were synthesized. The MOM-protected tripod **5**, where the phenol functionality is masked as an acetal, proved to be ideal. Reacting the trisaminoamide **3** with benzoyl chloride affords, after MOM cleavage, the trissalicylamide **8** in 29% overall yield.

The ferric complexes are prepared by mixing $[Fe(H_2O)_6](ClO_4)_3$ with the ligands **6** or **8** in DMF in the presence of NEt_3, yielding the corresponding Fe(III) complexes $[Fe^{III}(\mathbf{6}@\mathbf{OO})]$ **9** and $[Fe^{III}(\mathbf{8}@\mathbf{OO})]$ **10**. (For convenience, the coordination environment of the iron in the tripodal ligands is emphasized by @**OO** and @**NN** for salicylamide and bipyridine coordination respectively).

(15) Cohen, S. M.; Meyer, M.; Raymond, K. N. *J. Am. Chem. Soc.* **1998**, *120*, 6277.
(16) Bonardi, A.; Merlo, C.; Pelizzi, C.; Pelizzi, G.; Tarasconi, P.; Covatorta, F. *J. Chem. Soc., Dalton Trans.* **1991**, 1063.
(17) Stassinopoulos, A.; Schulte, G.; Papaefthymiou, G. C.; Caradonna, J. P. *J. Am. Chem. Soc.* **1991**, *113*, 8686.
(18) Lutz, A.; Ward, T. R.; Albrecht, M. *Tetrahedron* **1996**, *52*, 12197.
(19) Lutz, A.; Ward, T. R. *Helv. Chim. Acta* **1998**, *81*, 207.
(20) Lehn, J.-M. *Supramolecular Chemistry; Concepts and Perspectives.*; VCH: Weinheim, Germany, 1995.
(21) For a review see Boulas, P. L.; Gómez-Kaifer, M.; Echegoyen, L. *Angew. Chem., Int. Ed. Engl.* **1998**, *37*, 216.
(22) (a) Zelikovich, L.; Libman, J.; Shanzer, A. *Nature* **1995**, *374*, 790. (b) For a highlight on this work see Constable, E. C. *Nature* **1995**, *374*, 760. (c) Canevet, C.; Libman, J.; Shanzer, A. *Angew. Chem., Int. Ed. Engl.* **1996**, *35*, 2657.
(23) Belle, C.; Pierre, J.-L.; Saint-Aman, E. *New J. Chem.* **1998**, 1399.
(24) (a) Livoreil, A.; Dietrich-Buchecker, C. O.; Sauvage, J.-P. *J. Am. Chem. Soc.* **1994**, *116*, 9399. (b) Cárdenas, D. J.; Livoreil, A.; Sauvage, J.-P. *J. Am. Chem. Soc.* **1996**, *118*, 11980. (c) Zahn, S.; Canary, J. W. *Angew. Chem., Int. Ed. Engl.* **1998**, *37*, 305.
(25) De Santis, G..; Fabbrizzi, K.; Iacopino, D.; Pallavicini, P.; Perotti, A.; Poggi, A. *Inorg. Chem.* **1997**, *36*, 827.

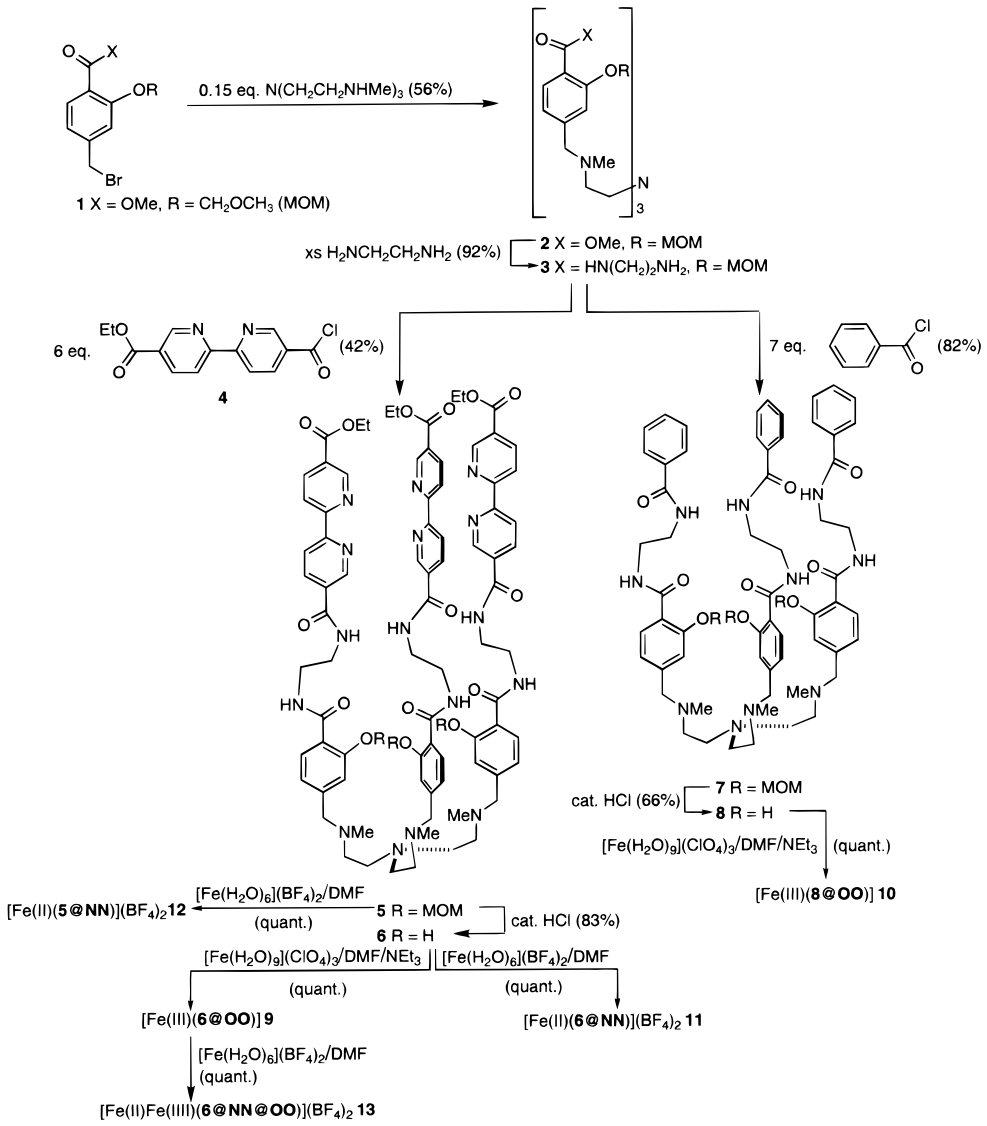

Figure 3. Synthesis of tripodal ligands **5**, **6**, and **8** and their corresponding complexes [Fe^{III}(**6**@**OO**)] **9**, [Fe^{III}(**8**@**OO**)] **10**, [Fe^{II}(**5**@**NN**)]$(BF_4)_2$ **12**, [Fe^{II}(**6**@**NN**)]$(BF_4)_2$ **11**, and [$Fe^{II}Fe^{III}$(**6**@**NN**@**OO**)]$(BF_4)_2$ **13**.

The ferrous complexes are prepared by mixing equimolar amounts of $[Fe(H_2O)_6](BF_4)_2$ and ligand **5** or **6** in DMF to afford [Fe^{II}(**5**@**NN**)]$(BF_4)_2$ **12** and [Fe^{II}(**6**@**NN**)]$(BF_4)_2$ **11**. The dinuclear compound [$Fe^{II}Fe^{III}$(**6**@**NN**@**OO**)]$(BF_4)_2$ **13** is readily synthesized by adding equimolar amounts of $[Fe(H_2O)_6](BF_4)_2$ to [Fe^{III}(**6**@**OO**)] **9** in DMF. All these complexes were characterized by cyclic voltammetry, electrospray MS, UV−vis spectroscopy, and combustion analysis.[26] To reduce the affinity of iron for the bipyridine moiety, electron-withdrawing ester/amide functionalities were incorporated at the 5,5′-positions. We speculated that this would decrease the stability constants as well as the oxidation potential of the ferrous complexes (vide supra). As a direct consequence thereof, both [Fe^{II}(**5**@**NN**)]$(BF_4)_2$ **12** and [Fe^{II}(**6**@**NN**)]$(BF_4)_2$ **11** display some high-spin character,[27] thus preventing their NMR characterization.

For the ferric complexes **9**, **10**, and **13**, elemental analysis as well as MS (negative ionization) revealed the presence of a counterion, suggesting that a proton resides in the electron-rich tetraamine cavity spanned by the Me_3TREN anchor.[15,29] Many other bases as well as Fe^{III} sources were tested, but in all cases the presence of one counteranion was revealed by combustion analysis.

In a crystallization attempt with [Fe^{II}(**6**@**NN**)]$(BF_4)_2$ **11** in DMF, we observed a slow color change from violet to orange, suggestive of iron oxidation and concomitant translocation into the **OO** cavity (vide supra). It is interesting to note that such a color change is not observed when either the MOM-protected complex [Fe^{II}(**5**@**NN**)]$(BF_4)_2$ **12** or the dinuclear complex [Fe^{II}-Fe^{III}(**6**@**NN**@**OO**)]$(BF_4)_2$ **13** is dissolved in DMF. This suggests that the phenol functionality in [Fe^{II}(**6**@**NN**)]$(BF_4)_2$ **11**, which is in part deprotonated (by some traces of dimethylamine

(26) Although IR spectroscopy has elegantly been applied by Raymond and co-workers to characterize the "salicylate binding mode" from protonated iron−enterobactin,[13] the carbonyl−amide region in our systems is too complex to unambiguously assign.

(27) James, B. R.; Parris, M.; Williams, R. J. P. *J. Chem. Soc.* **1961**, 4630; see also James, B. R.; Lyons, J. R.; Williams, R. J. P. *Biochemistry* **1962**, *1*, 379.

(28) The overall shape and maxima for complexes **9** and **10** as well as **11** and **12** are very similar; the extinction coefficients, however, differ. This may be caused by a slight change in ligand (L) conformation and is reflected in the Fe−L π-overlap, which in turn determines the intensity of the MLCT (or LMCT) transitions.

(29) Caravan, P.; Orvig, C. *Inorg. Chem.* **1997**, *36*, 236.

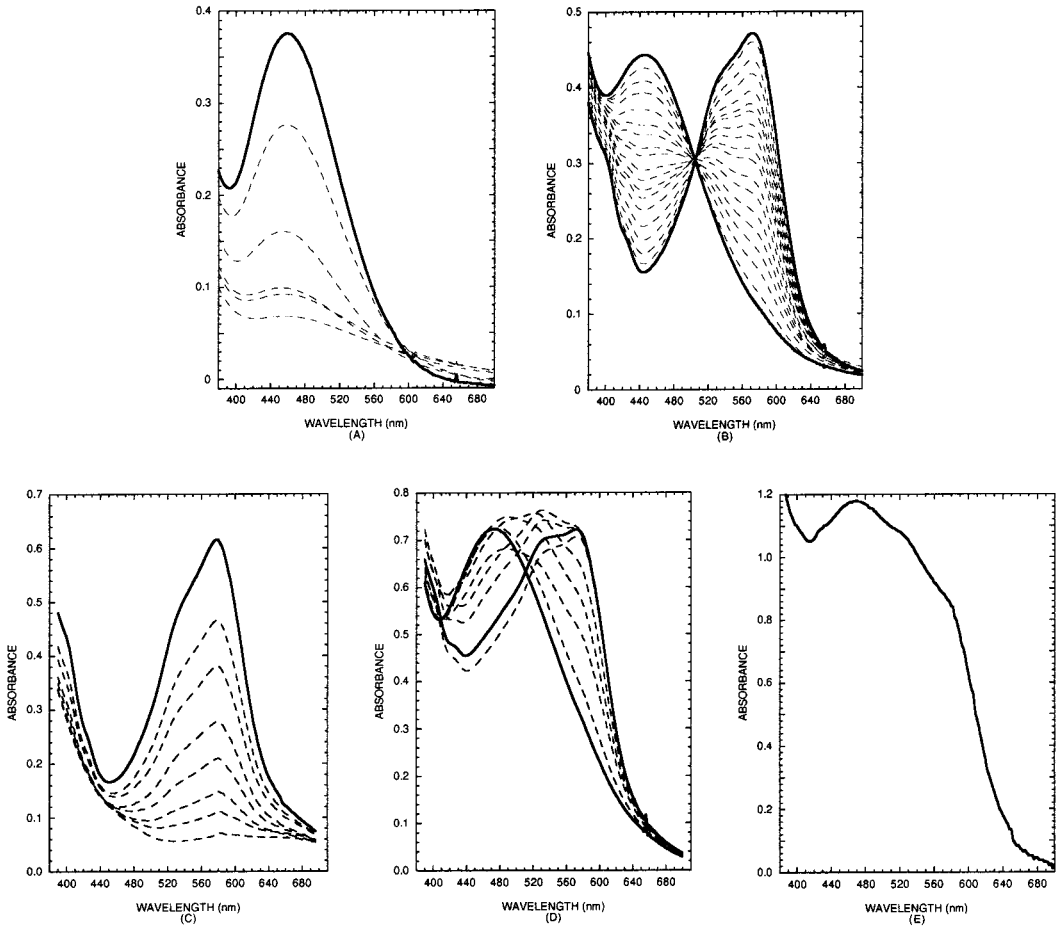

Figure 4. Visible absorption spectra resulting from treatment of [Fe^{III}(**8**@**OO**)] **10** with ascorbic acid (A), [Fe^{III}(**6**@**OO**)] **9** with ascorbic acid (B), [Fe^{II}(**5**@**NN**)]$(BF_4)_2$ **12** with H_2O_2 (C), [Fe^{II}(**6**@**NN**)]$(BF_4)_2$ **11** with $K_2S_2O_8$ (D), and [$Fe^{II}Fe^{III}$(**6**@**NN**@**OO**)]$(BF_4)_2$ **13** (no chemical treatment) (E).

Table 1. MLCT and LMCT Data for Complexes **9**−**13** in DMF

compound	λ_{max} (nm)	ϵ ($cm^{-1}\cdot M^{-1}$)
[Fe^{III}(**6**@**OO**)] **9**	460	3200
[Fe^{III}(**8**@**OO**)] **10**	460	2100
[Fe^{II}(**6**@**NN**)]$(BF_4)_2$ **11**	574, 543[a]	2300, 2250
[Fe^{II}(**5**@**NN**)]$(BF_4)_2$ **12**	576, 544[a]	1800, 1300
[$Fe^{II}Fe^{III}$(**6**@**NN**@**OO**)]$(BF_4)_2$ **13**	576, 524,[a] 470	2200, 2700, 3000

[a] Shoulder.

produced by the photochemical degradation of DMF), favors the iron translocation/oxidation process. Eventually, we found that the most reliable synthesis of [Fe^{III}(**6**@**OO**)] **9** is the O_2 oxidation of the ferrous complex [Fe^{II}(**6**@**NN**)]$(BF_4)_2$ **11** in DMF in the presence of NEt_3.

Visible Spectroscopy. As mentioned above, the color of the iron complexes varies from orange to violet for the ferric and ferrous complexes respectively, offering a straightforward visual indication of the metal's oxidation state and coordination environment. The position and molar absorption coefficients for the MLCT and LMCT maxima and shoulders of all complexes **9**−**13** are summarized in Table 1. As can be judged from Table 1, the optical spectra for [Fe^{III}(**8**@**OO**)] **10** and [Fe^{II}(**5**@**NN**)]$(BF_4)_2$ **12** are very similar to those of **9** and **11**, respectively. This strongly supports the assertion that the Fe^{III} indeed resides in the salicylamide cavity in [Fe^{III}(**6**@**OO**)] **9**. Similarly, the Fe^{II} is coordinated to the three bipyridine moieties in [Fe^{II}(**6**@**NN**)]$(BF_4)_2$ **11**. The reduced extinction coefficients observed for both ferrous complexes fully support the reduced Fe(II)−N bond strength (compared to $[Fe(bpy)_3]^{2+}$ $\epsilon_{523\ nm} = 9200$).[27,28]

Redox-Triggered Iron Translocation. Whether the tripodal ligands are hexadentate or dodecadentate has a dramatic effect on the redox behavior of the resulting complexes.

Treating the ferric complex devoid of bipyridines [Fe^{III}(**8**@**OO**)] **10** with aliquots of ascorbic acid results in a bleaching of the solution (Figure 4A). This suggests that the reduced species [Fe^{II}(**6**@**OO**)]$^-$ is unstable, eventually leading to a release of the ferrous ion, probably as $[Fe(DMF)_6]^{2+}$, which is colorless.

When a DMF/H_2O solution of [Fe^{III}(**6**@**OO**)] **9** is treated with ascorbic acid at room temperature (RT), the solution gradually turns violet, suggesting that the ferrous ion is released from the salicylate cavity and trapped by the bipyridines, producing [Fe^{II}(**6**@**NN**)]$(BF_4)_2$ **11**. The absorption spectra for the titration of [Fe^{III}(**6**@**OO**)] **9** with ascorbic acid are presented in Figure 4B. The presence of an isosbestic point at 510 nm suggests that only two species are in equilibrium, indicative of an intramolecular process.

Upon addition of aqueous H_2O_2 aliquots, the MLCT band of complex [Fe^{II}(**5**@**NN**)]$(BF_4)_2$ **12** disappears, suggesting that the [Fe^{III}(**5**@**NN**)]$^{3+}$ is unstable, eventually leading to an Fe^{3+} release (see Figure 4C).

When treated with H_2O_2 at RT, the violet solution of [Fe^{II}(**6**@**NN**)]$(BF_4)_2$ **11** gradually turns orange, eventually affording the ferric complex [Fe^{III}(**6**@**OO**)] **9**. Here again, the presence of an isosbestic point at 510 nm suggests an intramolecular process. The resulting spectra are nearly superimposable on those obtained for the reduction of [Fe^{III}(**6**@**OO**)] **9** with ascorbic acid. Interestingly, when potassium persulfate is used

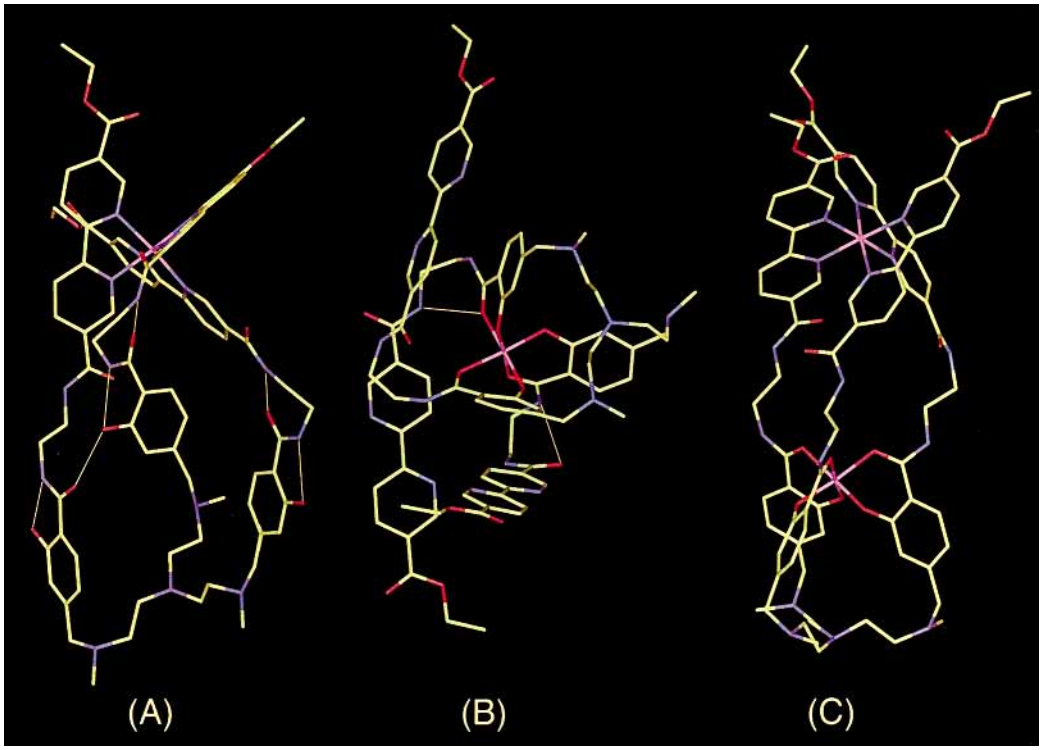

Figure 5. Extensible systematic force field optimized structure of $[Fe^{II}(\mathbf{6@NN})]^{2+}$ **11** (A), $[Fe^{III}(\mathbf{6@OO})]$ **9** (B), and $[Fe^{II}Fe^{III}(\mathbf{6@NN@OO})]^{2+}$ **13** (C) (hydrogen atoms were deleted for clarity; H-bonds are shown in yellow).

for the oxidation of $[Fe^{II}(\mathbf{6@NN})](BF_4)_2$ **11**, both starting and final spectra coincide with those obtained with H_2O_2. The "intermediate" spectra, however, do not display the characteristic isosbestic point (see Figure 4D); they resemble that of the bimetallic complex $[Fe^{II}Fe^{III}(\mathbf{6@NN@OO})](BF_4)_2$ **13** (Figure 4E).

Since, when persulfate is used as oxidizing agent, the dinuclear complex $[Fe^{II}Fe^{III}(\mathbf{6@NN@OO})](BF_4)_2$ **13** is produced, we conclude that the translocation is intermolecular. A possible explanation for the inter- vs intramolecular pathway for the translocation could arise from the products resulting from the reduction of H_2O_2 and $S_2O_8^{2-}$, respectively. In the former case, a strong base (OH^-) is produced; whereas in the latter, the weak base (SO_4^{2-}) is formed. The hydroxide readily deprotonates the phenolic functionality in $[Fe^{II}(\mathbf{6@NN})](BF_4)_2$ **11**, which favors Fe^{III} coordination at this site. With sulfate, the anion is much less basic and therefore does not fully deprotonate the phenolic functionality; the solvated ferric ions then diffuse out of the ligand cavity, eventually affording the dinuclear complex $[Fe^{II}Fe^{III}(\mathbf{6@NN@OO})](BF_4)_2$ **13** as intermediate.

Modeling Studies. Despite repeated efforts, we were not able to obtain suitable crystals for X-ray studies of any of the above complexes. Molecular modeling studies were thus undertaken to gain a detailed picture on the overall geometry of both ferric and ferrous complexes.

The extensible systematic force field (ESFF) code was used to optimize the gas-phase geometries of complexes $[Fe^{III}(\mathbf{6@OO})]$ **9**, $[Fe^{II}(\mathbf{6@NN})]^{2+}$ **11**, and $[Fe^{II}Fe^{III}(\mathbf{6@NN@OO})]^{2+}$ **13**.[30] Considering the abundance of amide functionalities and potential H-bonding sites in these complexes, an energy minimization scheme similar to that used for proteins was adopted. After optimization of an initial structure, the system was annealed at 1250 K for 200 ps. During this time, each 10 ps the obtained structure (yielding a total of 20 structures) was fully minimized to an energy gradient of 10^{-4} kcal·mol^{-1}·Å^{-1}.

Table 2. Structural Data for the ESFF Energy Minimization of Complexes **9** and **13**

	$[Fe^{III}(\mathbf{6@OO})]$ **9**	$[Fe^{II}Fe^{III}(\mathbf{6@NN@OO})]^{2+}$ **13**	X-rays[c]
$Fe-O_{phenol}$ (Å)	1.86	1.86	1.92
$Fe-O_{carbonyl}$ (Å)	2.02	2.02	2.08
Fe−N (Å)		2.08	
α[b] (deg)	63.58	60.00	60.02
salicylate twist[c] (deg)	9.93	12.32	18.26

[a] Averaged over the three structures published by Raymond and coworkers.[15] [b] Defined as the averaged trigonal twist angle. [c] Averaged $O_{carbonyl}-C_{carbonyl}-C_{phenol}-O_{phenol}$ dihedral angle.

As there is no crystal field stabilization energy for high-spin ferric complexes, the geometry around six-coordinate ferric ions can be either octahedral, trigonal prismatic, or anywhere between. The salicylamide chelate displays pronounced electronic asymmetry (phenolate oxygen vs carbonyl oxygen). As a consequence, the facial isomer is predicted to be preferred as it forces the phenolate oxygens (better donors) into an energetically favorable cis arrangement.[31] Thus, only *fac*-$[Fe^{III}(\mathbf{6@OO})]$ **9** was optimized. The annealing procedure yielded $[Fe^{III}(\mathbf{6@OO})]$ **9** with all *Z*-amides (average $Fe-O_{phenolate} = 1.86$ Å and $Fe-O_{carbonyl} = 2.02$ Å; see Figure 5 B and Table 2). The average trigonal twist angle $\alpha = 63.58°$ is diagnostic of a nearly perfect octahedral environment.[32,33] Only two hydrogen bonds are present in the optimized structure: $N_{bpy-amide}-H\cdots O_{carbonyl}$ of the salicylamide and $N_{salicylamide}-H\cdots O_{carbonyl}$ at the bipyridine

(30) Barlow, S.; Rohl, A. L.; Shi, S.; Freeman, C. M.; O'Hare, D. *J. Am. Chem. Soc.* **1996**, *118*, 7578.

(31) Albright, T. A.; Burdett, J. K.; Whangbo, M.-H. *Orbital Interactions in Chemistry*; John Wiley: New York, 1985.

(32) Karpishin, T. B.; Stack, T. D. P.; Raymond, K. N. *J. Am. Chem. Soc.* **1993**, *115*, 182.

side. Both these interstrand H-bonds force the diaminoethane spacers in a gauche conformation.

Comparing our results to three [Fe^{III}(salicylamide)$_3$] structures recently reported by Cohen et al.[15] (see Table 2), we note on average slightly shorter Fe−O bond lengths for our ESFF-optimized structures (see Table 2). The flexibility of the salicylamide chelates as defined by the twist angle of the salicylate chelate rings ($O_{carbonyl}-C_{carbonyl}-C_{phenol}-O_{phenol}$) is nicely reflected in the calculations. Similarily, the averaged trigonal twist angles are comparable.

In contrast to the salicylamide chelate, both donors in the bipyridine are essentially equivalent. The facial vs meridional preference is thus dictated by steric factors. Both *fac*-[Fe^{II}(**6**@**NN**)]$^{2+}$**11** and *mer*-[Fe^{II}(**6**@**NN**)]$^{2+}$**11** were minimized by the above procedure. After optimization, however, close inspection of the structures revealed that some of the bipyridine amides had an energetically unfavorable *E*-configuration.

A Cambridge Structural Database search of all primary arylamides showed that none of the >800 hits displayed an *E*-configuration. Therefore, the configuration of the amides was constrained (250 kcal·mol^{-1}·rad^{-2}) to *Z* during optimization. The annealing scheme described above was slightly modified as the temperature of each retained structure (20 in total as above) was *gradually* decreased from 1250 to 1 K within 10 ps (125 K·ps^{-1}). At 200 K, the constraints were removed to allow full relaxation of the amides. The 20 structures were fully minimized to an energy gradient of 10^{-4} kcal·mol^{-1}·Å^{-1}.

This procedure yielded minimized structures with *Z*-amides, which proved to be in all cases more stable than the previously minimized structures. The *fac*-[Fe^{II}(**6**@**NN**)]$^{2+}$**11** was computed to be 5.6 kcal·mol^{-1} more stable than the *mer*-[Fe^{II}(**6**@**NN**)]$^{2+}$**11** isomer. The optimized structure *fac*-[Fe^{II}(**6**@**NN**)]$^{2+}$**11** is depicted in Figure 5A. The computed Fe−N bond lengths (2.08 Å) are slightly longer than the Fe−N bond lengths for [Fe(bipyridine)$_3$]$^{2+}$ collected in the CSD (2.00 Å). Although probably accidental, it nicely reflects the weaker Fe−N bond strength imposed by the electron-withdrawing substituents on the bipyridines.

A total of six H-bonds are present in the minimized geometry, yielding an unsymmetrical structure as one of these is an intrastrand contact (between a salicylamide $O_{carbonyl}\cdots H-O_{phenol}$ of another strand). Forcing the ferrous complex into a C_3 symmetric structure yields a complex that lies 35.6 kcal·mol^{-1} higher in energy. Two H-contacts are found between salicylamide $O_{carbonyl}\cdots H-N_{bpy-amide}$, again forcing two of the diaminoethane spacers into a gauche conformation. As reported for the free enterobactin modeling studies,[34] all three salicylamide N−C−C−C_{OH} torsion angles are close to 0°, affording three H-contacts between $O_{phenol}\cdots H-N_{salicylamide}$.

The structure of the dinuclear complex [$Fe^{II}Fe^{III}$(**6**@**NN**@**OO**)](BF$_4$)$_2$ **13** was optimized with the Z-amide constraint. With two metals present, a nearly ideal C_3 symmetry is computed as can be appreciated from Figure 5C (see also Table 2 for metrical data). No hydrogen bonds are present in this rigid system.

From these modeling studies, it appears that the system must undergo significant reorganization upon iron translocation. In addition to $C_{sp^3}-C_{sp^3}$ bond rotations in both the spacer and the anchor to accommodate the incoming metal in an octahedral environment, we note that the salicylamide N−C−C−C_{OH} torsion angle must rotate from ∼0° (in [Fe^{II}(**6**@**NN**)]$^{2+}$ **11**, Figure 5A) to ∼180° in [Fe^{III}(**6**@**OO**)] **9** (Figure 5B). This allows the carbonyl oxygen to bind to the ferric ion, yielding a salicylamide chelate. Interestingly, a similar problem arises upon protonation of [Fe^{III}(enterobactin)]$^{3-}$ to yield [Fe^{III}(enterobactinH$_3$)] bound via three salicylamides, as can be appreciated from Figure 1C.[34]

We conclude that although the ligand is predisposed for selective binding and intramolecular translocation of iron,[35] improvement in the ligand design should yield preorganized devices with improved kinetic switching properties.

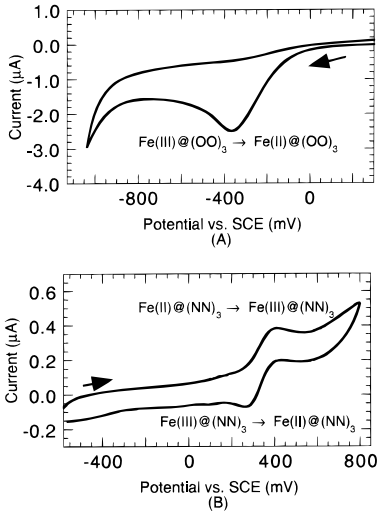

Figure 6. Cyclic voltammograms (vs SCE) of [Fe^{III}(**6**@**OO**)] **9** (A) and [Fe^{II}(**6**@**NN**)](BF$_4$)$_2$ **11** (B).

Table 3. Cyclic Voltammetric Data for Complexes **9**−**13**[a]

compound	E_p^{ox} (mV)[b]	E_p^{red} (mV)[b]	i_p^{ox}/i_{pred}
[Fe^{III}(**6**@**OO**)] **9**		−368	
[Fe^{III}(**8**@**OO**)] **10**		−424	
[Fe^{II}(**6**@**NN**)](BF$_4$)$_2$ **11**	+492	+387	1.14
[Fe^{II}(**5**@**NN**)](BF$_4$)$_2$ **12**	+478	+388	1.53
[$Fe^{II}Fe^{III}$(**6**@**NN**@**OO**)](BF$_4$)$_2$ **13**	+510[c]	+380[c]/−363	25.50[c]

[a] Scan rate 40 mV/s. [b] Referenced against SCE. [c] $Fe^{II/III}$@**NN** couple.

Electrochemistry. Cyclic voltammograms for all reported complexes **9**−**13** were recorded in *N*,*N*-dimethylformamide (DMF) electrolyte solutions (see the Experimental Section for details).

Regardless of the denticity of the tripodal ligands, both ferric complexes [Fe^{III}(**6**@**OO**)] **9** and [Fe^{III}(**8**@**OO**)] **10** behave similarly, displaying irreversible reduction waves at −368 and −424 mV, respectively. A typical cyclic voltammogram for complex [Fe^{III}(**6**@**OO**)] **9** is presented in Figure 6A. All relevant electrochemical data are collected in Table 3. It is instructive to compare the reduction potentials of the above ferric complexes with those of [Fe^{III}(enterobactin)]$^{3-}$ [although the experimental conditions differ (DMF vs H_2O)]. As outlined in the Introduction (see Figure 1), the reduction potential of [Fe^{III}(enterobactin)]$^{3-}$ lies outside the reducing power of natural reductants: $E_{1/2} = -1030$ mV at pH = 7.4.[36] Upon catecholate protonation and translocation into the salicylate binding mode, the reduction potential dramatically decreases, thus allowing reduction of the ferric ion in the salicylate cavity by NADH or

(33) A Cambridge Structural Database search revealed that trigonal prismatic environments are encountered with [Fe^{III}(O∧O)$_3$] complexes where (O∧O) is a bidentate ligand with two oxygen donor atoms displaying small bite angles (e.g., five-membered chelate rings).

(34) Shanzer, A.; Libman, J.; Lifson, S.; Felder, C. E. *J. Am. Chem. Soc.* **1986**, *108*, 7609.

(35) Blanc, S.; Yakirevitch, P.; Leize, E.; Meyer, M.; Libman, J.; Van Dorsselaer, A.; Albrecht-Gary, A.-M.; Shanzer, A. *J. Am. Chem. Soc.* **1997**, *119*, 4934.

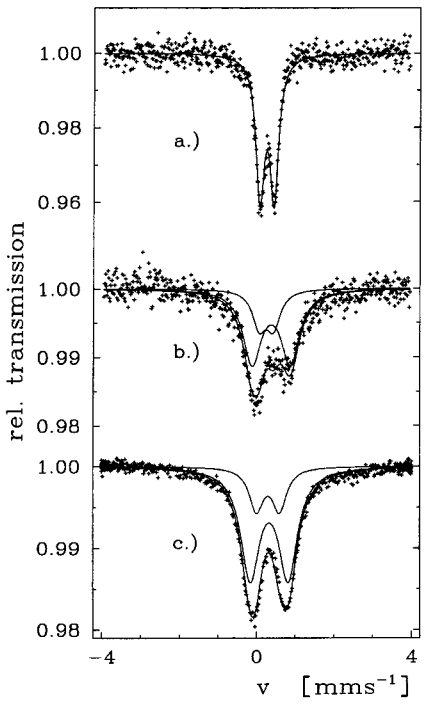

Figure 7. Mössbauer spectra of $[Fe^{II}(\mathbf{6}@\mathbf{NN})](BF_4)_2$ **11** (A), after flushing $[Fe^{II}(\mathbf{6}@\mathbf{NN})](BF_4)_2$ **11** with O_2 in DMF (B), and $[Fe^{III}(\mathbf{6}@\mathbf{OO})]$ **9** (C).

$FADH_2$ accompanied by a concomitant iron release from enterobactin.

The redox behavior of both ferrous complexes $[Fe^{II}(\mathbf{6}@\mathbf{NN})](BF_4)_2$ **11** and $[Fe^{II}(\mathbf{5}@\mathbf{NN})](BF_4)_2$ **12** is quasireversible (Figure 6B and Table 3). The equilibrium potentials lie at 439 and 433 mV, respectively. It appears that the Fe^{III} produced by oxidation of the Fe^{II} complexes remains in the bipyridyl environment and, under these experimental conditions, migrates only slowly to the salicylamide binding site. Reducing the scan rate, however, fails to produce any trace of $[Fe^{III}(\mathbf{6}@\mathbf{OO})]$ **9**. Instead, the intensity of the reduction wave gradually decreases to produce an nearly irreversible system. As in the case of the persulfate oxidation, we believe that since the phenol functionality is not fully deprotonated, the ferric ion diffuses away from the electrode. Such a situation is encountered for $[Fe^{II}Fe^{III}(\mathbf{6}@\mathbf{NN}@\mathbf{OO})](BF_4)_2$ **13** at all scan rates (10−400 mV/s), yielding large i_p^{ox}/i_p^{red} ratios.

Mössbauer Spectroscopy. Mössbauer spectroscopy is an ideal tool to probe the coordination environment and the oxidation state of iron. Unfortunately, due to the very limited solubility of the complexes, the Mössbauer spectra were recorded on powder samples, rather than on solutions.

The ferrous complex $[Fe^{II}(\mathbf{6}@\mathbf{NN})](BF_4)_2$ **11** was submitted to Mössbauer spectroscopy. The obtained data ($\delta = 0.36$ mm·s^{-1} and $\Delta E_Q = 0.37$ mm·s^{-1}) support a trisbipyridyl environment for low-spin ferrous ion (compare with $\delta = 0.35$ mm·s^{-1} and $\Delta E_Q = 0.40$ mm·s^{-1} for $[Fe(bpy)_3]^{2+}$),[37] as shown in Figure 7a.

(36) As suggested by a referee, to compare the reduction potentials in DMF of complexes **9** and **10** with the reduction potential of [Fe^{III}-(enterobactin)] in water, $E_{1/2}$ of ferrocene (a solvent independent species) was used as a reference: E_p^{red} $[Fe^{III}(\mathbf{6}@\mathbf{OO})]$ **9** −368 mV vs SCE, −780 mV vs ferrocene; E_p^{red} $[Fe^{III}(\mathbf{8}@\mathbf{OO})]$ **10** −424 mV vs SCE −836 mV vs ferrocene; E_p^{red} $[Fe^{III}$(enterobactin)] at pH 7.4, −1058 mV vs SCE, −1246 mV vs ferrocene. See Lee, C.-W.; Ecker, D. J.; Raymond, K. N. *J. Am. Chem. Soc.* **1985**, *107*, 6920.

(37) For example see Decurtis, S.; Schmalle, H. W.; Schneuwly, P.; Ensling, J.; Gütlich, P. *J. Am. Chem. Soc.* **1994**, *116*, 9521.

Table 4. Protonation Constants (log *K*) of Ligands **6** and **8** at 25.0 °C and $I = 0.05$ M (NaCl) in 70% (w/w) 1,4-Dioxane/Water[a]

protonation site	ligand **8**	ligand **6**
TREN N	10.64 (1)	11.0 (1)
TREN N	9.94 (1)	10.1 (1)
TREN N	9.11 (1)	9.4 (1)
phenolate O	7.37 (2)	7.9 (1)
phenolate O	6.14 (2)	6.7 (1)
phenolate O	5.79 (1)	5.8 (1)
bpy N		5.4 (1)
bpy N		<2
bpy N		<2
pH range	2.5−11.5	2.5−11.7

[a] Standard deviations are given in parentheses.

To elucidate the translocation mechanism, a DMF solution of $[Fe^{II}(\mathbf{6}@\mathbf{NN})](BF_4)_2$ **11** was flushed with O_2 for 3 h. The resulting reddish-purple solution was taken to dryness and submitted to Mössbauer spectroscopy. The resulting Mössbauer spectrum is presented in Figure 7b. The asymmetric doublet can be fitted by a superposition of two doublets. The doublet with the smaller quadrupole splitting is identical with that of the pure low-spin ferrous complex $[Fe^{II}(\mathbf{6}@\mathbf{NN})](BF_4)_2$ **11**. The main component displays a quadrupole pair with $\delta = 0.49$ mm·s^{-1} and a quadrupole splitting $\Delta E_Q = 0.99$ mm·s^{-1}, assigned to the ferric complex $[Fe^{III}(\mathbf{6}@\mathbf{OO})]$ **9**. These data are very similar to those obtained by Pecoraro et al.[11] for protonated ferric enterobactin: a pH-dependent analysis of ferric enterobactin suggests that, below pH 4, the iron resides in a trissalicylamide environment [Fe(enterobactinH_3)] (isomer shift $\delta = 0.50$ mm·s^{-1} and a quadrupole splitting $\Delta E_Q = 0.8$ mm·s^{-1}).[11]

Flushing with oxygen for an additional hour the above ferric/ferrous sample in a 1:1 DMF/NEt_3 mixture yields a red solution that, after filtration and solvent removal, was submitted to Mössbauer spectroscopy (Figure 7c). The slight asymmetry of the doublet suggests the presence of two different high-spin ferric species. The dominating doublet is identical with that of the previous sample ($\delta = 0.49$ mm·s^{-1}, $\Delta E_Q = 0.99$ mm·s^{-1}). The Mössbauer parameters of the second doublet component ($\delta = 0.42$ mm·s^{-1}, $\Delta E_Q = 0.60$ mm·s^{-1}) point toward the presence of some ferric oxyhydroxide.[38]

The Mössbauer data thus strongly support Raymond's proposal for a salicylate binding mode in [Fe(enterobactinH_3)] at low pH. The formation of FeO(OH) upon raising the pH suggests that the binding strength of salicylamide ligands toward Fe^{III} is too small to prevent hydrolysis at physiological pH. To gain further insight, we determined the stability constant of $[Fe^{III}(\mathbf{8}@\mathbf{OO})]$ **10**.

Stability Constants. The slow decomposition of DMF in basic medium prohibits its use in potentiometric titrations. Thus, different water/organic solvent mixtures (MeOH, DMSO, DMF, and 1,4-dioxane) were tested. Eventually a 70% (w/w) 1,4-dioxane/water mixture (ionic strength 0.05 M NaCl) proved most suitable, despite very limited solubility of ligand **6**. (See the Experimental Section for details.)

Protonation Constants. The protonation constants of ligands **6** and **8** are listed in Table 4. For the MOM-protected ligand **5**, the three log *K* values [7.27(1), 6.10(1), and 5.69(1)] in the range pH 2.7−8.0 show good agreement with the corresponding data obtained for ligands **6** and **8**. This fully supports the assumption that the MOM-protecting group hydrolyzes under acidic condi-

(38) Greenwood, N. N.; Gibb, T. C. *Mössbauer Spectroscopy*; Chapman and Hall Ltd.: London, 1971.

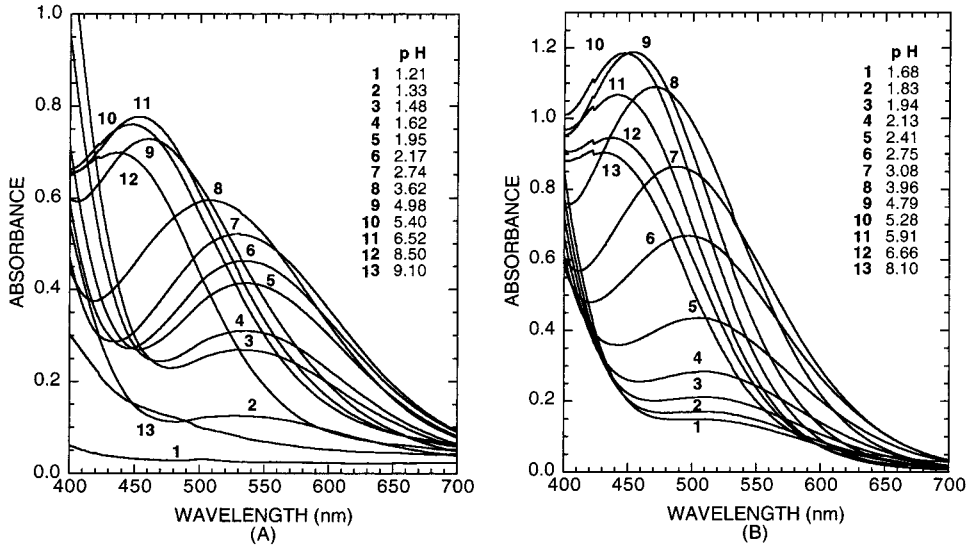

Figure 8. Visible absorption spectra of Fe^{III} ligand **6** ($c_M = 0.61$ mM, $c_L = 0.91$ mM) at different pH values (A) and Fe^{III} ligand **8** (c_M 1.04 mM, $c_L = 1.17$ mM) at different pH values (B).

tions, yielding free phenolic groups in the acidic samples before titration. Ligand **5** was thus not investigated further.

Although ligand **6** has as many as 10 protonation sites (three 2,2′-bipyridine type N, three phenolate O^-, and four TREN N), only seven measurable deprotonation processes were found in the pH range studied. Ligand **8** on the other hand has six measurable log *K* values.

By analogy to other TREN-based ligands,[39,40] one of the four amines has low basicity, while the remaining three have log *K* values in the normal range for aliphatic amines (9−11). Recent studies on related tripodal aminocarboxylate ligands based on TREN suggest that it is the apical nitrogen which has the least basic character, and this is most likely the case for ligands **5**, **6**, and **8**.[41]

Because ligand **8** lacks the bpy units, the three lower log *K* values must belong to the phenolate oxygens and the three higher to the TREN nitrogens. The comparison of these data with the corresponding values for ligand **6** strongly suggests that only one of the bpy nitrogens is protonated in the latter under these experimental conditions, even with a 10-fold excess of acid. To support this argument, the protonation constant of the free 2,2′-bipyridine was determined in this solvent mixture to be log $K = 3.14(1)$, which is significantly smaller than the corresponding value in water (4.40).[39] This less pronounced basic character of the bpy nitrogens may be responsible for the lack of the protonation of all the bpy units in ligand **6**. Due to the very limited solubility of ligand **6**, the determined protonation constants have a higher than usual error.

Complex Formation of [Fe^{III}(8@OO)] 10. At the onset of the titration, the samples [Fe^{III}(**6**@**OO**)] **9** and [Fe^{III}(**8**@**OO**)] **10** are deep purple and cherry red, respectively. Between pH 4 and 5, both samples turn to orange-red. Upon further increasing the pH, the samples become pale yellow. By pH 7, the samples are essentially colorless as the metal ion hydrolyzes. Although several models including di- and monoprotonated species of the phenolate part of the ligand or mixed hydroxo complexes with different stoichiometries were considered, our attempts to fit the titration curves with ligand **6** were not as successful as in the ligand **8** systems. The reason for this is most probably the extensive hydrolysis of Fe(III), dictated by the very low concentrations due to poor solubility. We thus focus on ligand **8**, which is significantly more soluble in this solvent mixture.

Table 5. Complex Formation (Log β_{pqr}) and Derived Equilibrium Constants for the Fe(III)−Ligand **8** System at 25.0 °C and $I = 0.05$ M (NaCl) in 70 % (w/w) 1,4-Dioxane/Water[a]

	p	*q*	*r*	pH potentiometry	vis spectrophotometry
$[Fe(\mathbf{8}H_5)]^{5+}$	1	1	5	50.18 (1)	51.1 (1)
$[Fe(\mathbf{8}H_4)]^{4+}$	1	1	4	47.91 (1)	48.3 (1)
$[Fe(\mathbf{8}H_3)]^{3+}$	1	1	3	44.58 (1)	44.3 (1)
$pK[Fe(\mathbf{8}H_5)]^{5+}$				2.27	2.8
$pK[Fe(\mathbf{8}H_4)]^{4+}$				3.33	4.0
pH range				2.2−4.0	1.4−6.0

[a] Standard deviations are given in parentheses.

The best fit was obtained in the Fe(III)−ligand **8** system by considering the model presented in Table 5.

The visible spectrophotometric titrations of the samples containing Fe(III)−ligand **6** or **8**, respectively, show very similar behavior. The results of the spectrophotometric titration curves of the Fe(III)−ligand **6** samples at 1:1 metal ion-to-ligand ratio are displayed in Figure 8A. The spectra exhibit a charge-transfer band at 535 nm (purple complex). The absorbance values increase in the range pH 1.5−3.9 and show a continuous shift to 450 nm up to pH 5.5. Upon raising the pH further, this band disappears. The ligand **8** system displays strikingly similar features (Figure 8B), exhibiting a charge-transfer band at 515 nm (cherry-red complex), which shifts to 450 nm with increasing pH.

The results of the evaluation of the spectrophotometric data for the Fe(III)−ligand **8** system are presented in Table 5. The spectrophotometric titration confirms the model obtained by potentiometry, as the stability data determined by the two different methods are in good agreement. It has to be mentioned that the ϵ_{max} values for the complexes formed are close to each other (in the range 1700−2200 mol^{-1} dm^3 cm^{-1}). Therefore, the calculated stability data from the spectrophotometric measurements have higher uncertainty than those of potentiometry.

(39) Pettit, G.; Pettit, L. D. *IUPAC Stability Constants Database*; IUPAC/Academic Software: Otley, U.K., 1993.
(40) Caravan, P.; Hedlund, T.; Liu, S.; Sjöberg, S.; Orvig, C. *J. Am. Chem. Soc.* **1995**, *117*, 11230.
(41) Geraldes, C. F. G. C.; Brücher, E.; Cortes, S.; Koenig, S. H.; Sherry, A. D. *J. Chem. Soc., Dalton Trans.* **1992**, 2517.

Again here, for solubility reasons, all our efforts to obtain quantitative data with the Fe(III)−ligand **6** system were unsuccessful.

Both pH potentiometry and spectroscopic titration data yield similar results for the stability constant of [Fe^{III}(**8**@**OO**)] **10**. On the basis of their stoichiometry and formation pH range, the [Fe(**8**H_5)]$^{5+}$, [Fe(**8**H_4)]$^{4+}$, and [Fe(**8**H_3)]$^{3+}$ species may contain one to three deprotonated salicylamide unit(s) coordinated to the metal ion. This assumption is supported by literature data on related tripodal ligands capable of forming salicylamide-type complexes. For example, the purple (λ_{max} = 492 nm) iron(III) complex of MESAM [*N*,*N*′,*N*″-tris(2-hydroxybenzoyl)-1,3,5-tris(aminomethyl)benzene] is thought to have one or two protonated salicylamide arms.[13] The deprotonation of this species results in the formation of an orange-colored (λ_{max} = 468 nm) trissalicylamide-type complex. A further proof is the p*K* values of the [Fe(**8**H_5)]$^{5+}$, [Fe(**8**H_4)]$^{4+}$ species (Table 5). The comparison of these values with the p*K* values of the free ligand corresponding to the deprotonation of the phenolic groups indicates the metal ion-promoted, enhanced deprotonation of the phenolic groups in the complex. Ligand **8** seems to be effective in Fe^{III} binding in the acidic pH range; however, it is not able to prevent the hydrolysis of the metal ion in basic medium, thus confirming the Mössbauer data.

The calculated stability constants for the direct formation process of the trissalicylamide complex [Fe^{III}(**8**@**OO**)] **10**: Fe^{3+} + H_3**8** = [Fe(**8**H_3)]$^{3+}$ is log *K* = 44.58 − 10.64 − 9.94 − 9.11 = 14.89. For comparison the corresponding stability constants were calculated for tripodal enterobactin model compounds capable of salicylamide-type Fe^{III} binding.[5,42,43] The data (log *K*) (MECAMS, 19.6; CYCAMS, 21.5; LICAMS, 21.0) for the Fe^{3+} + H_3L → FeH_3L reaction are significantly larger than for [Fe^{III}(**8**H_3@**OO**)] **10**. This equilibrium definition eliminates considerable uncertainty from the high protonation constants of these catechol derivatives; however, the Fe^{3+} complexes of the catechol derivatives are still more stable than [Fe(**8**H_3)]$^{3+}$ by 5−7 orders of magnitude. The recently published stability constant (log β_{110} = 25.34) for TRENSAM capable only of pure trissalicylamide type Fe^{III} binding is considerably larger as well.[15] These variations may lie in the different experimental conditions [70% (w/w) dioxane/water vs water] but can more likely be attributed to the less favorable formation of the [Fe(**8**H_3)]$^{3+}$ complex because of the flexibility of TREN backbone in the ligand.

On the basis of their analogous structures and the similarity of their pH potentiometric and visible spectroscopic features (compare Figure 8 spectra a and b), the iron binding capabilities of ligands **6** and **8** toward Fe^{III} are expected to be very similar. The rather small stability constant allows the metal to readily take part in a redox-mediated iron translocation, rationalizing both the cyclic voltammetry data and the formation of FeO(OH) upon raising the pH.

Conclusions

The synthesis and characterization of tripodal dodecadentate ligands incorporating three salicylamide and three bipyridine binding sites as well as iron complexes thereof are reported. In the presence of a single iron, it was shown that these dodecadentate ligands are coded for oxidation state-selective iron chelation and intramolecular iron transport. The low-spin ferrous ion binds selectively to the soft trisbipyridine pocket, while the high-spin ferric ion binds to the harder trissalicylamide pocket. Moreover, it was observed that oxidation or reduction induces intramolecular (depending on conditions), reversible iron translocation between these two sites, thus revealing switchlike properties. It should be stressed, however, that this switching process is critically dependent on the pH. The oxidation requires basic conditions, favoring deprotonation of the phenol functionality, resulting in an intramolecular iron translocation. The reduction, in contrast, requires acidic conditions to reprotonate the free phenolate sites. This device could thus be regarded as an X(N)OR logic gate[44] that responds to *two* chemical stimuli: redox and pH.

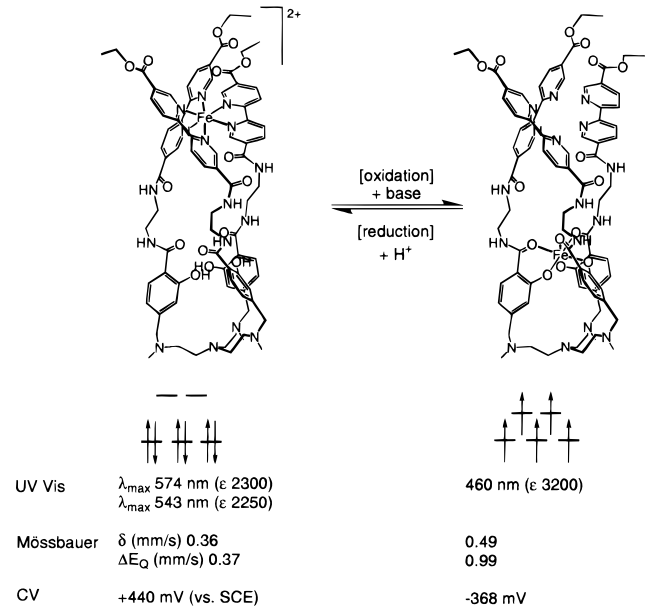

Figure 9. Summary of the spectroscopic data of [Fe^{II}(**6**@**NN**)]$^{2+}$ **11** and [Fe^{III}(**6**@**OO**)] **9**.

The iron localization, oxidation state, and translocation are conveniently addressed by visible spectroscopy. Cyclic voltammetry reveals an irreversible [Fe^{III}(**6**@**OO**]/[Fe^{II}(**6**@**OO**)]$^-$ redox couple and a quasireversible [Fe^{II}(**6**@**NN**)]$^{2+}$/[Fe^{III}(**6**@**NN**)]$^{3+}$ couple. The Mössbauer data for [Fe^{III}(**6**@**OO**)] **9** fully support Raymond's suggestion that, upon lowering the pH, the iron in [Fe^{III}(enterobactin)]$^{3-}$ translocates into the so-called salicylate binding mode. The small stability constant determined for [Fe^{III}(**8**@**OO**)] **10** (log *K* = 14.89) is reflected in its reduction potential (E_p^{red} = −424 mV), thus suggesting that, after catecholate protonation and translocation into the salicylate binding mode, [Fe^{III}(enterobactinH_3)] can be reduced, if necessary, by natural reducing agents. A summary of spectroscopic data for complexes [Fe^{III}(**6**@**OO**)] **9** and [Fe^{II}(**6**@**NN**)]$(BF_4)_2$ **11** is presented in Figure 9.

Molecular modeling on [Fe^{III}(**6**@**OO**)] **9** and [Fe^{II}(**6**@**NN**)]$(BF_4)_2$ **11** reveals that the system described herein is predisposed but not preorganized to act as an intramolecular switch. Possible improvements include introduction of a rigid spacer between the salicylamide and bipyridine binding sites, as well as capping to afford macrobicyclic systems. Preliminary kinetic analysis indicates that the redox/translocation process occurs on a 10 s time scale. Stopped-flow analysis is currently underway to elucidate the translocation mechanism.

(42) Harris, W. R.; Carrano, C. J.; Cooper, S. R.; Sofen, S. R.; Avdeef, A. E.; McArdle, J. V.; Raymond, K. N. *J. Am. Chem. Soc.* **1979**, *101*, 6097.

(43) Harris, W. R.; Raymond, K. N.; Weitl, F. L. *J. Am. Chem. Soc.* **1981**, *103*, 2667.

(44) Credi, A.; Balzani, V.; Langford, S. J.; Stoddart, J. F. *J. Am. Chem. Soc.* **1997**, *119*, 2679.

Experimental Section

General. All reactions were carried out under nitrogen by standard Schlenk techniques. All solvents were dried according to standard procedures. All chemicals were purchased from either Fluka AG Buchs or Aldrich and used as received. The synthesis of compounds **1**−**6** has been described elsewhere.[18] Instruments and conditions were as follows: Mass spectra, electrospray ionization (ESMS) Fisons VG; LSIMS, AutoSpec Q VG (dithiothreitol/dithioerythritol 5:1 matrix); UV−vis spectra, Hewlett-Packard 8452 A diode-array spectrophotometer, wavelengths in nanometers, extinction coefficient ϵ in square centimeters per mole, sh = shoulder; NMR spectra, Bruker AC 300, ^{13}C (75 MHz) and ^{1}H (300 MHz) referenced against residual solvent peaks. Elemental analyses were performed at Novartis Basel and samples were equilibrated in air to a constant weight.

Electrochemistry. Cyclic voltammograms were acquired under N_2 in DMF with a 0.01 M *n*-Bu_4NBF_4 supporting electrolyte. A platinum disk working electrode, a platinum plate counterelectrode, and an Ag wire pseudoreference electrode were used. A cyclic voltammogram $TCNQ/TCNQ^{\bullet -}$ was used to reference all the data versus SCE [$E_{1/2}$-($TCNQ/TCNQ^{\bullet -}$) = 0.28 V vs SCE in DMF).[45] The data were collected with the general purpose electrochemical system (GPES 3.2 from Echo Chemie) on an Autolab PSSTAT10 connected to a PC. The data were treated on a Macintosh with KaleidaGraph 3.0.4 (Abelbeck Software).

Mössbauer Spectra. A constant-acceleration type Mössbauer spectrometer together with a 1024-channel analyzer operating in the time scale mode was employed. The source, ^{57}Co/Rh, was kept at RT for all measurements. Spectra of the samples were collected at 100 K by means of a He continuous-flow cryostat. The Mössbauer spectra were fitted by the transmission integral method of the program MOSFUN.[46] Isomer shift values are reported with respect to the standard α-Fe at RT.

Potentiometric and Spectrophotometric Measurements. All the equilibrium measurements were carried out in a 70% (w/w) 1,4-dioxane/water mixture at an ionic strength of 0.05 M (NaCl). Potentiometric measurements of the ligands in the absence, and presence, of Fe^{III} were performed with a Fisher Acumet 950 pH-meter equipped with a Metrohm combined glass electrode. The electrode system was calibrated before each measurement by titrating a known amount of HCl in the solvent mixture with a known concentration of NaOH. The base solution with a concentration of ca. 0.05 M was made in the above solvent mixture. A plot of millivolts (measured) vs pH (calculated) gave a working slope and intercept so that the pH could be read as $-\log [H^+]$ directly. The pK_w value in 70% (w/w) 1,4-dioxane/water was determined to be 15.56(1). A Metrohm Dosimat 665 automatic buret was used for the base additions, and the buret and pH meter were interfaced to a PC such that each titration was automated. The temperature of the solutions was kept constant at 25.0 ± 0.1 °C by a Julabo UC circulating bath. The electrode was stored in the solvent mixture between measurements.

NaOH solutions (0.05 M) were prepared from dilution of saturated (50%) aqueous NaOH with freshly boiled, distilled water and freshly opened high-purity 1,4-dioxane, both flushed with argon before use. The NaOH solutions were standardized potentiometrically against potassium hydrogen phthalate. Aqueous $FeCl_3$ was prepared from $FeCl_3 \cdot 6H_2O$ by dissolving in 0.1 M HCl. After reduction with $SnCl_2$, the metal ion concentration of the solution was determined by titration with potassium permanganate. The excess acid was calculated by titrating with standard NaOH and analyzing the titration curve by the Gran method.[47]

Ligand protonation constants were determined from titration of 10.0 mL samples over the pH range 2.0−11.7. The ligand concentrations ranged from 0.4 to 3.0 mM depending upon the solubilities. The metal−ligand solutions were titrated up to pH 8 or until slow processes occurred (10 min being not enough to reach the pH equilibrium), indicative of the metal ion hydrolysis. The ratio of the metal ion to ligand used was between 1:1 and 1:2, with the ligand concentration in the range 0.4−2.5 mM.

The protonation constants and the purity of the ligands were determined by using the program SUPERQUAD[48] that iteratively varies the stability constants to minimize the sum of the squares of the differences between observed and calculated pH values.[49] The protonation constants (log K_i) refer to the following equilibria: $H^+ + L^{n-} = HL^{(n-1)-}$, $H^+ + HL^{(n-1)-} = H_2L^{(n-2)-}$, etc. In all the calculations considered, $\chi^2 < 8.0$ and $\sigma < 0.9$.

Attempts to calculate concentration stability constants ($\beta_{pqr} = [M_pL_qH_r]/[M]^p[L]^q[H]^r$) from the potentiometric data in the Fe^{III}−ligand **8** and **6** systems were performed with the aid of the PSEQUAD computer program. During the calculations the following Fe(III)−hydroxo complexes were assumed:[50] $[Fe(OH)]^{2+}$ (log $\beta_{1,0,-1} = -2.45$), $[Fe(OH)_2]^+$ (log $\beta_{1,0,-2} = -6.03$), $[Fe(OH)_3]$ (log $\beta_{1,0,-3} = -12.32$), $[Fe_2(OH)_2]^{4+}$ (log $\beta_{2,0,-2} = -2.84$), and $[Fe_3(OH)_4]^{5+}$ (log $\beta_{3,0,-4} = -6.11$).

Electronic absorption spectra were recorded on a Shimadzu UV-2100 or Hewlett-Packard 8453 instrument in Fe^{III}−ligand **8** or **6** systems with 1.00 cm path length quartz cells. The complex formation was studied in two ways. In the first method, 12−15 samples were prepared having the same metal ion and ligand concentrations with different pH values ranging from 1.5 to 9.0. In the second method, samples with 1:1.1 metal ion-to-ligand ratio were titrated with base in the pH range 1.8−9.0 under argon and the visible spectra were recorded.

The spectrophotometric data were fitted with the PSEQUAD program.[49] The program uses the mass balance equations of the components and calculates the concentration stability constants ($\beta_{pqr} = [M_pL_qH_r]/[M]^p[L]^q[H]^r$) of the absorbing species. The calculations were made with the absorbance data in the 400−600 nm range at 15−18 different wavelengths.

During the calculations with PSEQUAD volumes of the titrant were fitted in the case of the pH−potentiometric data and absorbance values of the spectrophotometric titration curves. Accepted fittings (the average difference in the calculated and experimental titration curves expressed in cubic centimeters of the titrant and in absorbance values, respectively) were below 1×10^{-2} in the former cases and below 2×10^{-2} in the latter ones.

Synthesis of 5′,5‴,5⁗,5⁗′-[Nitrilotris[2,1-ethandiyl(methylimino)-methylene-[2-(methoxymethoxy)-4,1-phenylene]carbonylimino(2,1-ethandiyl)iminocarbonyl]]trisbenzol 7. The triamine **3** (480 mg, 0.54 mmol) and triethylamine (0.78 mL, 5.63 mmol) were dissolved in dichloromethane (250 mL). Benzoyl chloride (0.43 mL, 3.75 mmol) in dichloromethane (100 mL) was slowly added. The resulting solution was stirred overnight and solvents were evacuated under reduced pressure. The resulting solid was column-chromatographed with dichloromethane−methanol−aqueous ammonia (25%) 100:7:1, affording a colorless oil (530 mg, 0.44 mmol, 82%). ^{1}H NMR (CD_3OD): 2.14 (s, 9 H, NCH_3), 2.45−2.51 (m, 6 H, CH_2), 2.62−2.64 (m, 6 H, CH_2), 3.42 (s, 6 H, NCH_2), 3.48 (s, 9 H, OCH_3), 3.53−3.59 (m, 12 H, CH_2CH_2), 5.24 (s, 6 H, OCH_2), 7.00 (br s, 3 H, aromatic H), 7.12 (br s, 3 H, aromatic H), 7.42−7.46 (m, 6 H, benzylic H), 7.49−7.52 (m, 3 H, benzylic H), 7.71 (d, J = 7.8 Hz, 3 H, aromatic H), 7.84−7.85 (m, 6 H, benzylic H), 8.33 (br s, 3 H, NH), 8.59 (br s, 3 H, NH). ^{13}C NMR (CD_3OD): 39.4 and 39.7 ($OCNHCH_2CH_2NHCO$), 40.5 (NCH_3), 46.0 (CH_2CH_2), 56.3 (OCH_3), 61.5 (NCH_2), 94.7 (OCH_2), 127.5 (dI), 128.7, 130.8, 131.6, 134.7, 154.9 (aromatic C), 169.2, 169.8 (CO). MS (LSIMS): 1209.6 (28), 239.1. Anal. Calcd ($C_{66}H_{84}N_{10}O_{12}$): C, 65.54; H, 7.00; N, 11.58. Found: C, 65.36; H, 7.05; N, 10.46.

Synthesis of 5′,5‴,5⁗,5⁗′-[Nitrilotris[2,1-ethandiyl(methylimino)-methylene[2-hydroxy-4,1-phenylene]carbonylimino(2,1-ethandiyl)-iminocarbonyl]]trisbenzol 8. The MOM-protected tripod **7** (530 mg, 0.44 mmol) was dissolved in ethanol (200 mL), and 32% HCl (0.10

(45) Tsubata, Y.; Suzuki, T.; Miyashi, T. *J. Org. Chem.* **1992**, *57*, 6749.
(46) Müller, W. *MOSFUN − Mössbauer Spectra Fitting Program for Universal Theories, Description and User's Guide*; Müller, W., Ed.: Institut für Anorganische Chemie und Analytische Chemie, Johannes Gutenberg-Universität: Mainz, Germany, 1980.
(47) Gran, G. *Acta Chem. Scand.* **1950**, *4*, 559.
(48) Gans, P.; Sabatini, A.; Vacca, A. *J. Chem. Soc., Dalton Trans.* **1985**, 1195.
(49) Zékány, L.; Nagypál, I. *Computational Methods for the Determination of Stability Constants*; Legett, D., Ed.; Plenum: New York, 1985.
(50) Baes, C. F.; Mesmer, R. E. *Hydrolysis of Cations*; Wiley-Interscience: New York, 1976.

mL) was added. The solution was heated under reflux overnight and the solvents were evaporated under reduced pressure. The solid was column-chromatographed with dichloromethane−methanol−aqueous ammonia (25%) 100:13:1 to yield a colorless foam (310 mg, 0.29 mmol, 66%). ^{1}H NMR (CD_3OD): 2.20 (s, 9 H, NCH_3), 2.45 (t, J = 6.8 Hz, 6 H, CH_2), 2.66 (t, J = 6.8 Hz, 6 H, CH_2), 3.42 (s, 6 H, NCH_2), 3.58−3.62 (m, 12 H, CH_2CH_2), 6.74 (dd, J = 8.1 and 1.6 Hz, 3 H, aromatic H), 6.84 (d, J = 1.4 Hz, 3 H, aromatic H), 7.39−7.43 (m, 6 H, benzylic H), 7.47−7.51 (m, 3 H, benzylic H), 7.70 (d, J = 8.1 Hz, 3 H, aromatic H), 7.78−7.81 (m, 6 H, benzylic H). ^{13}C NMR (CD_3OD): 38.7 and 39.5 (OCNH*C*H_2*C*H_2NHCO), 41.6 (NCH_3), 51.3 and 53.2 (*C*H_2*C*H_2), 61.5 (NCH_2), 115.0, 118.3, 118.9, 126.8, 127.8, 128.1, 131.2, 134.1, 143.6, 161.0 (aromatic C), 169.2, 169.8 (CO). MS (LSIMS): 1077.20 (91). Anal. Calcd ($C_{60}H_{72}N_{10}O_9\cdot 2H_2O$): C, 64.73; H, 6.88; N, 12.58. Found: C, 64.86; H, 6.95; N, 12.05.

Synthesis of [Fe^{III}(6@OO)] 9. The ferrous complex [Fe^{II}(**6**@**NN**)]-$(BF_4)_2$ **11** (413.60 mg, 23.50 μmol) was dissolved in DMF (7 mL) and flushed with O_2 for 3 h. NEt_3 was added (0.32 mL, 2.36 mmol) and the orange solution was stirred an additional hour. Reverse filtration into Et_2O (40 mL) affords, after filtration, the ferric complex [Fe^{III}-(**6**@**OO**)] **9** in quantitative yield. MS (ESMS): 1580.50 ([ML − 3H]$^+$), 791.25 ([ML − H]$^{2+}$). Vis (DMF): 460 (3200). Anal. Calcd ($C_{81}H_{87}$-$FeN_{16}O_{15}\cdot 8H_2O\cdot HBF_4$): C, 53.68; H, 5.73; N, 12.37; B, 0.6; Fe, 3.08. Found: C, 53.86; H, 5.59; N, 12.96; B, 0.81; Fe, 3.20.

Synthesis of [Fe^{III}(8@OO)] 10. The trissalicylamide ligand **8** (111 mg, 0.103 mmol) and $[Fe(H_2O)_9](ClO_4)_3$ were dissolved in DMF (10 mL). After being stirred for 1 h at RT, NEt_3 (57 μL, 0.412 mmol) was added and the solution was stirred for an additional 3 h. Reverse filtration into Et_2O (200 mL) affords, after filtration, the ferric complex [Fe^{III}(**8**@**OO**)] **10** in quantitative yield. MS (LSIMS): 1126.3 ([ML-3H]$^+$) 1077.9 ([L]$^+$), 613.1 ([ML-3H]$^{2+}$). Vis (DMF): 460 (2100). Anal. Calcd ($C_{60}H_{69}FeN_{10}O_{13}\cdot 5H_2O\cdot HClO_4$): C, 54.6; H, 6.0; N, 10.6; Fe, 4.2. Found: C, 54.25; H, 6.06; N, 10.89; Fe, 3.84.

Synthesis of [Fe^{II}(6@NN)](BF$_4$)$_2$ 11. The dodecadentate ligand **6** (194.00 mg, 0.13 mmol) was suspended in a DMF (15 mL) and nitromethane (10 mL) mixture. After the suspension was briefly heated, $[Fe(H_2O)_6](BF_4)_2$ (42.86 mg, 0.13 mmol) was added and the violet solution was stirred overnight at RT. Volatiles were evaporated in vacuo and the solid was dissolved in nitromethane. After filtration with a filter stick (reverse filtration), the solvent was removed in vacuo to afford the ferrous complex [Fe^{II}(**6**@**NN**)]$(BF_4)_2$ **11** (184.00 mg, 0.11 mmol, 82%). MS (ESMS): 1669.95 ([ML-BF_4]$^+$), 1527.99 ([L]$^+$), 791.48 ([ML-2BF_4]$^{2+}$), 764.50 ([L]$^{2+}$). Vis (DMF): 574 (2300), 543 (2250). Anal. Calcd ($C_{81}H_{90}B_2F_8FeN_{16}O_{15}\cdot 6H_2O$): C, 52.15; H, 5.51; N, 12.00; B, 1.16; F, 8.15; Fe, 2.99. Found: C, 51.66; H, 5.28; N, 12.22; B, 1.27; F, 8.22; Fe, 2.89.

Synthesis of the MOM-Protected Complex [Fe^{II}(5@NN)](BF$_4$)$_2$ 12. The MOM-protected tripodal ligand **5** (201.80 mg, 0.16 mmol) was suspended in nitromethane (40 mL). After the suspension was briefly heated, $[Fe(H_2O)_6](BF_4)_2$ (41.04 mg, 0.16 mmol) was added. The resulting violet solution was stirred overnight at RT and concentrated to 5 mL, at which point a precipitate began to form. The turbid solution was overlayered with diethyl ether (50 mL) and allowed to diffuse for 3 days. The microcrystalline solid was collected by reversed filtration, washed three times with Et_2O, and dried in vacuo, affording [Fe^{II}(**5**@**NN**)]$(BF_4)_2$ **12** in quantitative yield. MS (ESMS): 1669.95 ([ML − BF_4]$^+$), 1527.99 ([L]$^+$), 791.48 ([ML − 2BF_4]$^{2+}$), 764.50 ([L]$^{2+}$). Vis (DMF): 576 (1800), 544 (sh 1300). Anal. Calcd ($C_{87}H_{102}B_2F_8$-$FeN_{16}O_{18}\cdot 3H_2O$): C, 53.77; H, 5.60; N, 11.53; B, 1.11; F, 7.82; Fe, 2.87. Found: C, 53.43; H, 5.49; N, 11.28; B, 1.32; F, 8.10; Fe, 2.81.

Synthesis of [Fe^{II}Fe^{III}(6@NN@OO)](BF$_4$)$_2$ 13. The ferric complex [Fe^{III}(**6**@**OO**)] **11** (176.51 mg, 98.20 μmol) was dissolved in DMF (3 mL) and $[Fe(H_2O)_6](BF_4)_2$ (33.14 mg, 98.20 μmol) was added. After stirring for 3 h at RT, the solution was reverse-filtered in Et_2O (20 mL). The reddish solid was filtered, repeatedly washed with Et_2O, and dried in vacuo to afford [Fe^{II}Fe^{III}(**6**@**NN**@**OO**)]$(BF_4)_2$ **13** in quantitative yield. MS (ESMS): 1581.80 ([FeL − 2H]$^+$), 1527.66 ([L]$^+$), 818.50 ([Fe_2L − 3H]$^{2+}$), 795.51 ([L + Na + K]$^{2+}$), 791.57 ([FeL − 2BF_4]$^{2+}$), 764.52 ([L + 2H]$^{2+}$). UV (DMF): 576 (2200), 524 (sh 2700) 470 (sh 3000). Anal. Calcd ($C_{81}H_{87}B_2F_8Fe_2N_{16}O_{15}\cdot 10H_2O\cdot HBF_4$: C, 46.82; H, 5.23; N, 10.78; B, 1.56; Fe, 5.37. Found: C, 46.30; H, 5.16; N, 11.41; B, 1.55; Fe, 5.30.

Acknowledgment. This work was supported by the Swiss National Science Foundation. T.R.W. thanks the Stiftung für Stipendien auf dem Gebiete der Chemie for financial support (award of a Werner Fellowship to T.R.W. 1993−1999), Novartis for elemental analyses, Professor A. Ludi for his hospitality as well as S. Duclos, A. Daridon, and Dr. R. Kissner for help with cyclic voltammetry. P.B. and C.O. greatefully acknowledge the Natural Sciences and Engineering Research Council of Canada for a NATO Science Fellowship (1996−1998) and a research grant, respectively. We thank the referees for their insightful and constructive comments.

IC990225E